Agricultural and Forest Meteorology 330 (2023) 109311

Contents lists available at ScienceDirect

Agricultural and Forest Meteorology

journal homepage: www.elsevier.com/locate/agrformet

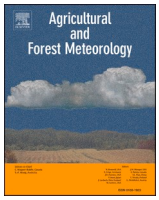

Bidirectional reflectance factor measurement of conifer needles with microscopic spectroscopy imaging

Yongkang Lai [a], Xihan Mu [a,*], Yuequn Bian [a], Xiaohan Dong [b], Feng Qiu [c], Xinyu Bo [a], Zhixiang Zhang [a], Yi Li [a], Xinli Liu [a], Linyuan Li [d], Donghui Xie [a], Guangjian Yan [a]

[a] State Key Laboratory of Remote Sensing Science, Institute of Remote Sensing Science and Engineering, Faculty of Geographical Science, Beijing Normal University, Beijing 100875, China
[b] College of Geoscience and Surveying Engineering, China University of Mining and Technology, Beijing 100083, China
[c] International Institute for Earth System Science, Nanjing University, Nanjing 210023, China
[d] College of Forestry, Beijing Forestry University, Beijing 100083, China

ARTICLE INFO

Keywords:
Conifer needles
Needle reflectance
Bidirectional reflectance factor (BRF)
Hyperspectral imaging
Microscopy imaging
Chlorophyll content

ABSTRACT

Leaf reflectance is widely used to retrieve leaf chlorophyll content (Cab) and parameterize canopy radiative transfer models. Measurements of broadleaf reflectance are typically made by using integrating sphere devices, but the approach is generally limited in conifer needle measurements due to the narrow needle coverage relative to the sample port of the integrating sphere. In this study, we proposed a method to measure the bidirectional reflectance factor (BRF) of needles by integrating a hyperspectral imaging spectrometer and an optical microscope. Pure needle pixels can be easily extracted from hyperspectral images after microscope magnification. The method was first validated by the narrow strips of broad leaves as proxies of needles, resulting in the difference between the measured BRF of strips and the BRF of whole broad leaves in the visible bands (400–700 nm) and in the near-infrared bands (700–1000 nm) being 0.0043 and 0.019, respectively. The method was also indirectly verified by tracking the variation in the natural needle BRF with its Cab, resulting in the change in BRF being consistent with the change in Cab. In addition, linear relationships between the needle Cab and the classic vegetation indices (*i.e.*, the red-edge simple ratio and normalized difference vegetation index) calculated from the BRF were found. Apart from the above, we found that (1) the BRF of the abaxial side has a discrepancy with that of the adaxial side of needles, (2) the BRF of a needle varies with its azimuth, hence affecting the correlation between vegetation indices and Cab, and (3) filtering the specular reflection on the microsurfaces of the needle could enhance the correlation between the vegetation indices and needle Cab. The method is expected to accurately measure the BRF of needles and hence to improve the applications of needle optical properties in plant sciences, ecology, and remote sensing fields.

1. Introduction

There are more than 600 coniferous species on Earth (Farjon 2010), which are widely distributed on the Earth's surface, especially in the high latitudes of the Northern Hemisphere. Due to the advantages of remote sensing technology, such as fast and large-scale imaging, remote sensing is considered the most convenient and effective method for monitoring coniferous forests. Remotely sensed signals are jointly influenced by canopy structure and optical properties of leaf and soil background. Leaf reflectance, as an input parameter, is vital for the calibration and validation of canopy reflectance models. Thus, the reflectance of conifer leaves (called needles) is indispensable to a better understanding of the remote sensing response from coniferous forests (Ramsey and Rangoonwala 2004). Additionally, leaf reflectance is the result of the interaction of various pigments and complex structures in leaves and has been used to describe leaf biophysical and biochemical properties (Carter et al., 1989; Fourty et al., 1996; Gausman et al., 1970). The spectral reflectance of the needle is of considerable interest for remote sensing applications (Middleton et al., 1997), such as tree species classification (Ramsey and Rangoonwala 2004), radiative transfer modeling for biophysical parameters of coniferous forest at the scale of leaf or canopy (Di Vittorio 2009), and leaf chlorophyll content

* Corresponding author.
E-mail address: muxihan@bnu.edu.cn (X. Mu).

https://doi.org/10.1016/j.agrformet.2023.109311
Received 22 March 2022; Received in revised form 3 January 2023; Accepted 4 January 2023
Available online 10 January 2023

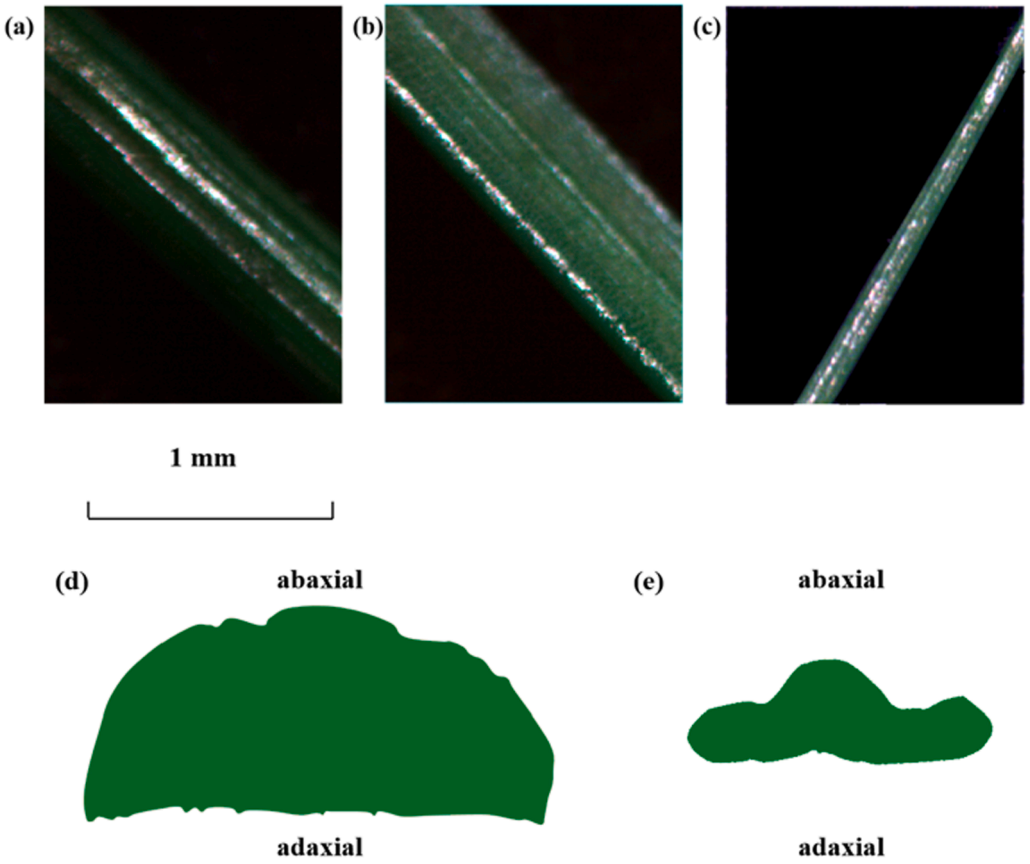

Fig. 1. True-color images of (a) the abaxial and (b) adaxial sides of a Scotch pine needle, and (c) the abaxial side of a larch needle. The images were taken by an imaging spectrometer coupled with a microscope. Bright spots on the needles were caused by specular reflection. Cross-sectional schematics of (d) the Scotch pine needle and (e) the larch needle. The widths of the needles of Scotch pine and larch were approximately 2 mm and 1 mm, respectively.

inversion (Gitelson et al., 2003; Gitelson et al., 2006; Li et al., 2019; Schlemmer et al., 2013).

The reflectance factor (RF) is obtained in the measurement, which means the ratio of signal observed from the target to that observed from an ideal Lambertian surface (usually called reference panel) under the same view and illumination conditions (Nicodemus et al., 1977; Schaepman-Strub et al., 2006). There are rigorous methods for measuring broadleaved RF, *i.e.*, an integrating sphere or a leaf clip coupled with a spectroradiometer (Li et al., 2019; Middleton et al., 1997; Yanez-Rausell et al., 2014a). Because the size of the needle (*e.g.*, the larch needle is approximately 1 mm) is too small to completely cover the sample port (*e.g.*, 10 mm) of the integrating sphere or the leaf clip, the method for measuring broadleaved RF cannot be directly used to measure the RF of needles (Hovi et al., 2020; Ramsey and Rangoonwala 2004; Rautiainen et al., 2018). Since it is a great challenge to obtain reliable RF spectra for needles (Hovi et al., 2020; Yanez-Rausell et al., 2014b), many efforts have been made to measure needle RF. To date, these methods can be generally classified into three categories. The first method measures the RF of the needle matrix formed by laying needles side by side (Daughtry and Biehl 1984; Gates et al., 1965). This method requires no gaps among needles forming the matrix. The second method measures the total signal reflected by multiple needles and background and then calculates the ratio of the gap areas among needles to the area of the field of view (Daughtry et al., 1989). Daughtry et al. calculated the gap fraction as the ratio of flux at 680 nm transmitted through the sample port with needles painted black compared with without needles in place. Since the needles have to be completely blacked out, it is considerably difficult to measure the gap fraction in this way. The second method was subsequently improved by improving the gap fraction calculation (Mesarch et al., 1999; Middleton et al., 1997), such as calculating the gap fraction with image classification. The third method proposed by Harron and Miller (1995) employs a sample holder specially made of two black anodized plates with independent slots. Each slot held a needle while measuring. Since the sample holder is also illuminated by light during the measurements, this method requires eliminating the influence of the sample holder to calculate the needle RF. These three methods have been widely used for decades (de Marín et al. 2016; Malenovský et al., 2006; Moorthy et al., 2008; Moorthy et al., 2004; Ramsey and Rangoonwala 2004; Zhang et al., 2008), yet there are still some drawbacks. For the first method, to ensure that there is no gap among the needles, it is often necessary to stack the needles in several layers to form the matrix. This is not only labor-intensive and time-consuming but also inaccurate for the measurement due to the multiple scattering between needles, especially for the near-infrared bands. For the second method, accurate measurement of the gap fraction is still difficult (Yanez-Rausell et al., 2014b). Moreover, the uncertainty of measured RF is dependent on the gap fraction (Ramsey and Rangoonwala 2004). Smaller gap fractions (0.10–0.15) are recommended to measure stable results (Mesarch et al., 1999). However, keeping the gap fraction within this range is difficult in practice, and the small gap fraction can lead to large multiple scattering effects. The third method requires specially made sample holders for different needle species so that the slots can fit the needles well. However, the production of sample holders is very time-consuming and labor-intensive. Additionally, the third method suffers from the attenuation of signal due to the presence of the sample holder (Wang et al., 2020).

With the development of imaging spectrometers, they are widely used in field spectral measurements of broad leaves (Ling et al., 2017; Zhang et al., 2015) and forest canopies (Li et al., 2021). Optical microscopes are frequently used to observe tiny objects. Currently, many

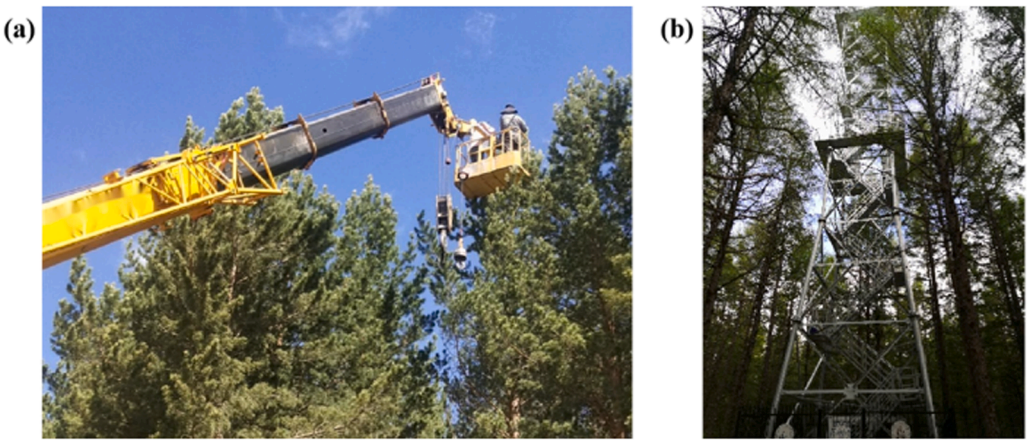

Fig. 2. Illustrations of (a) the crane and (b) the observation tower used to collect needle samples.

hyperspectral imaging spectrometers can be easily installed on ordinary optical microscopes (Zhang et al., 2019). Combining the imaging capabilities of the imaging spectrometer with the magnification capabilities of the microscope may allow direct measurement of the RF of an individual needle. In this study, we measure the bidirectional reflectance factor (BRF) of needles by coupling a ground-based imaging spectrometer and an optical microscope with natural or artificial light source (hereafter called the microscopy imaging method). Actually, the quantity measured with natural light source is hemispherical-directional reflectance factor, because even under clear conditions there is some hemispherical incoming radiation component. However, considering the hemispherical component in clear conditions is small, we also refer to the quantity measured under clear conditions as BRF.

This paper is organized as follows. In Section 2, the materials and methods are introduced. The experimental materials include sycamore (*Platanus orientalis* Linn.) leaves and needles of larch (*Larix principis-rupprechtii* Mayr.) and Scotch pine (*Pinus sylvestris* L. var. *mongolica* Litv.). Sycamore leaves are used to produce narrow strips (to simulate needles) to verify the accuracy of the method. In Section 3, we analyze and discuss the measurement results. In Section 4, the conclusion is presented.

2. Materials and methods

2.1. Overview of materials and methods

Firstly, the BRF of strips cut off from sycamore leaves was measured to demonstrate the necessity of microscopy in measuring the BRF of small leaves and the accuracy of the microscopy imaging method. Next, the BRF of larch needles and of Scotch pine needles under natural light and artificial light were measured. The processing steps including pixel extraction and RF calculation were designed to obtain the BRF of the samples (*i.e.*, strips of sycamore leaves and natural needles). Additionally, we measured the chlorophyll content (denoted Cab hereafter) of larch needles and of Scotch pine needles to analyze its relationship with two simple and widely used vegetation indices (*i.e.*, the red-edge simple ratio and modified normalized difference) calculated with the measured BRF of needles.

2.2. Experimental materials

2.2.1. Narrow strips of broad leaves

The sycamore leaves were picked at the Beijing Normal University campus, Beijing, China, on October 17, 2020. The sycamore leaves were placed into sealable plastic bags. The time for transporting sycamore leaves from picking locations to the measuring site was less than 5 min. Strips of 1–2 mm width and 3 cm length were cut off from the sycamore leaves to simulate needles. Thick veins were avoided when cutting off strips. A total of six strips were obtained.

2.2.2. Conifer needles

The natural needles were taken from larch and Scotch pine at Chengde, Hebei Province, China. The average heights of seven Scotch pine trees and five larch trees at the sampling sites were 13.77 m and 16.10 m, respectively. The widths of the needles of larch and Scotch pine were approximately 1 mm and 2 mm, respectively. The conifer needles of both Scotch pine and larch are bifacial leaves. The true-color images and cross-sections of a Scotch pine needle and a larch needle are shown in Figs. 1(a) – (e). The larch needles were picked on May 30, 2021, and September 15, 2021. The Scotch pine needles were picked on May 30, 2021, and September 16, 2021. As a deciduous tree species, larch has a growth period in May and a deciduous period in September. As an evergreen tree species, the leaves of Scotch pine do not fall all at once. Instead, less than one third of Scotch pine needles are shed every autumn, and new needles grow next summer.

A crane (Fig. 2(a)) and an observation tower (Fig. 2(b)) were used to obtain needle samples from different vertical layers. The needle samples of Scotch pine contained new needles (< 1 year old) and old needles whereas the needle samples of larch only contained new needles. The needle samples from the top and middle parts of the canopy were measured in May and the those from the top, middle, and lower parts of the canopy were measured in September. The twigs instead of needles were cut off from the tree to keep the needles fresh for a longer time. Experimenters stood on the crane or observation tower and cut off the twigs around the tower with a high branch cutter. The heights of the top, middle, and lower cutting twigs were 1.5 m, 6 m, and 12 m away from the crown top, respectively. Twenty-four twigs (12 top twigs and 12 middle twigs) were cut from seven Scotch pine trees and five larch trees on May 30. Three twigs (one in each layer) were cut from a Scotch pine and from a larch in September. The twigs were placed in sealable bags, and then the bags were placed into foam boxes with ice. The time for transporting samples from picking locations to the measuring site was less than 40 min. Scotch pine needles can sometimes be very curved. We chose the relatively straight needles when measuring. Twenty-eight needles of Scotch pine and twenty needles of larch were obtained in the experiment on May 30. Nine Scotch pine needles and ten larch needles were obtained in the experiment in September.

2.3. Measurement of BRF spectra, chlorophyll content and vegetation indices of needles

2.3.1. Measuring instruments

A push-broom Hyperspectral Imaging System, SOC710-VP (Surface Optics Corporation, USA), was used to collect BRF spectra. The SOC710-

Table 1
Characteristics of SOC710-VP.

Parameter	Value
Spectral Range (nm)	400–1000
Spectral Resolution (nm)	4.69
Number of Channels	128
Bit Depth (bit)	12
Cube Rate (s)	23.2
Integration Time (ms)	0–100

VP consists of a visible-to-near infrared spectrometer (400–1000 nm), low-noise silicon-based charge coupled device (CCD), and integrated scanning system. The characteristics of SOC710-VP are presented in table 1. The integration time of the instrument can be adjusted according to the light intensity to avoid the digital number (DN) value of the image being greater than the maximum value, *i.e.*, 2^{12}. The SOC710-VP automatically removes the dark current. This instrument can be easily installed on a c-mount trinocular microscope (Shanghai Meimei Metering Electricity Technology Co., Ltd. Shanghai, China). The microscope used in this study has a maximum magnification of 20 × . The spatial resolution of the SOC710-VP coupled with the microscope can reach 0.025 mm. The combined equipment was used to take a hyperspectral image of a standard reference panel made of polytetrafluoroethylene (Lambertian surface with a reflectance of 50%) to analyze whether the combination of microscope and SOC710-VP would cause the vignetting effect. The pixel values at the edge of the hyperspectral image of the reference panel were basically the same as the pixel values in the middle of the hyperspectral image, indicating that the combination of the microscope and the imaging spectrometer in this study did not cause the vignetting effect.

A hand-held Chlorophyll Content Meter-300 (Opti-Sciences CCM-300, Hudson, NH, USA) was used to measure the Cab of needle samples. CCM-300 uses the ratio of chlorophyll fluorescence emission at 735 nm and 700 nm (F735/F700) to measure the Cab. The CCM-300 adopts an artificial light source with the peak wavelength of 460 nm and a half band width of 15 nm. It measures chlorophyll fluorescence emission in two different wavelength ranges at the same time, *i.e.*, from 730 nm to 740 nm, and from 700 nm to 710 nm. The readings of this instrument are the ratio F735/F700, and the Cab is calculated according to the linear relationship between F735/F700 and laboratory-measured Cab (Gitelson et al., 1999). Since the relationship could vary with plant species, the original equation to calculate Cab from F735 /F700 was recalibrated for larch and Scotch pine separately with Cab measured using the solvent extraction methodology described in Moorthy et al. (2008). The equations of the Cab (units $\mu g \cdot cm^{-2}$) for larch and Scotch pine are, respectively,

$$Cab = 65.98 \cdot F735/F700 - 35.57 \quad (1)$$

$$Cab = 80 \cdot F735/F700 - 23 \quad (2)$$

2.3.2. Measurement of narrow strips of broad leaves

The hyperspectral images of the whole sycamore leaves and narrow strips were obtained on October 17, 2020, under clear and windless weather. The images of samples were taken on the roof of a building on the campus of Beijing Normal University. The view on the roof was open, and no other buildings blocked the sun. When taking hyperspectral images vertically downward, the whole leaf or narrow strips were placed on a 100% cotton fabric in black with low reflectance (*i.e.*, less than 0.03 in the visible band and less than 0.09 in the near-infrared band) to reduce the influence of multiple scattering between the samples and the background. The distance between the objective lens and the sample was adjusted so that the sample was clearly imaged in the scope of the imaging spectrometer. First, a hyperspectral image of each whole sycamore leaf was taken using the SOC710-VP to obtain reference values for the BRF of narrow strips. After measuring whole leaves, narrow strips (1–2 mm in width; 3 cm in length) were cut off. Then, hyperspectral images of the strips were taken with and without a microscope to demonstrate the necessity of microscopy in measuring the BRF of small leaves. Each whole leaf and its corresponding three strips are called a replicate of samples hereafter. Two replicates of samples were formed from two sycamore leaves. The narrow strips were flat and were marginally affected by multiple scattering when measuring narrow strips at the same time. Therefore, three narrow strips from the same sycamore leaf were measured together. To calculate the BRF of whole leaves and narrow strips, an image of the standard reference panel (Lambertian surface) was taken for each replicate of samples. The reference panel was placed horizontally on the black cloth to reduce the influence of possible vicinity effects. It took approximately 50 s to take an image with the hyperspectral imaging spectrometer and two minutes to complete the measurement of a replicate of samples.

2.3.3. Measurement of conifer needles under natural light

The measurement was taken under clear and windless weather on May 30. The measurement site was an open space with no trees or houses blocking the sun. The solar zenith angles (θ_s) when measuring Scotch pine needles and larch needles were approximately 30° and 45°,

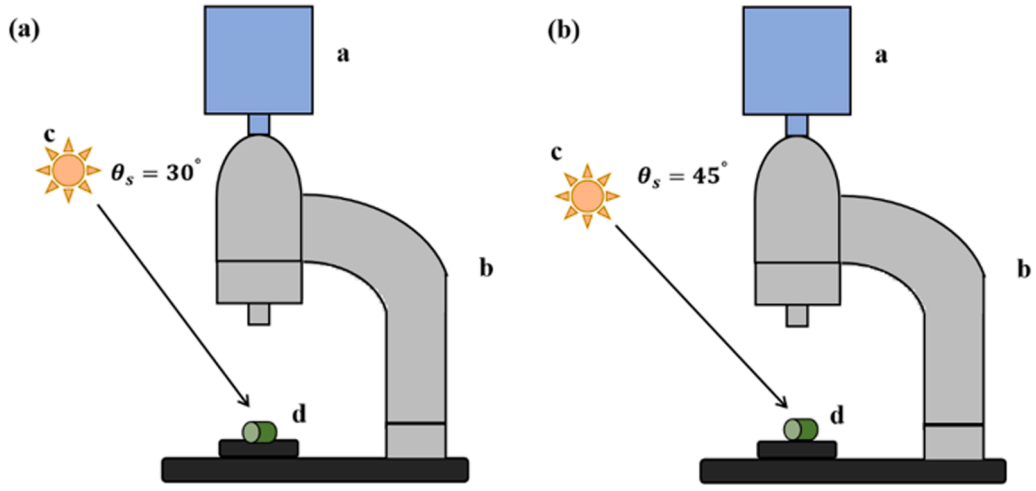

Fig. 3. Diagrams of the measurements of (a) Scotch pine needles and (b) larch needles. The a, b, c, and d in the diagrams represent the imaging spectrometer, microscope, sun, and needle, respectively. The azimuth of the needle is perpendicular to the azimuth of the sun. The solar zenith angles (θ_s) when measuring Scotch pine needles and larch needles were approximately 30° and 45°, respectively.

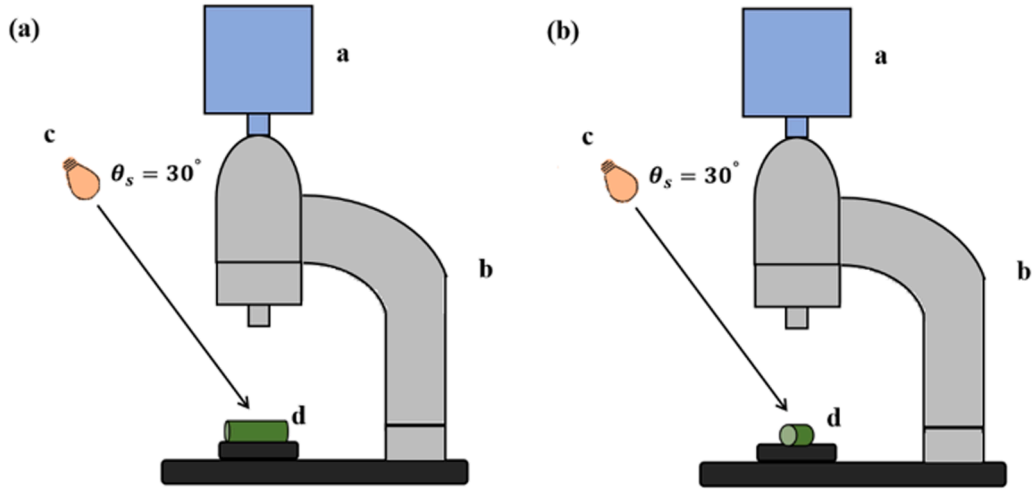

Fig. 4. Diagram of the two placement methods of larch needles. (a) The azimuth of the larch needle is consistent with the azimuth of the light source. (b) The azimuth of the larch needle is perpendicular to the azimuth of the light source. The a, b, c, and d in the diagrams represent the imaging spectrometer, microscope, artificial light, and needle, respectively. The zenith angle of the artificial light (θ_s) was approximately 30°.

respectively. (Fig. 3). Before each time a hyperspectral image was taken for needles, an image was taken for the standard reference panel. The needles were detached from the twigs before the measurement. Sixteen Scotch pine needles and ten larch needles were used to measure BRF. Similar to the narrow strips, when the images of the adaxial side of needles were taken, the needles were placed on a 100% cotton fabric in black. Since the abaxial side of the needles was rounded, the needle was pinned to the black cloth with two small pushpins. The distance between the objective lens and the sample was adjusted so that the needle sample was clearly imaged in the scope of the imaging spectrometer. The azimuth of the needle was perpendicular to the azimuth of the sun. The needles were individually photographed to prevent the influence of multiple scattering between them.

The CCM-300 was used to measure the Cab of the adaxial sides of the remaining 12 Scotch pine needles and 10 larch needles while measuring the BRF of needles with the SOC710-VP and microscope. The needles used to measure BRF and Cab were not exactly the same needles but on the same twigs.

2.3.4. Measurement of natural needles under artificial light

The weather was cloudy on September 15 and 16. Thus, needle samples obtained on September 15 and 16 were measured indoors. It was dark outside at the time of measurement, which was approximately one and a half hours after picking the twigs. Before the measurement, twigs were stored in ice-filled foam boxes. An artificial collimating halogen lamp (XD-301, Shanghai Meimei Metering Electricity Technology Co., Ltd. Shanghai, China) was used to simulate sunlight as the light source. The power and maximum illuminance of the lamp are 150 W and 160,000 lux, respectively. The illuminance of the lamp was adjusted to ensure that the DN value of the image did not exceed or even approach the maximum value. The use of high illuminance could make the temperature of the light source high and cause the light intensity to be unstable. The zenith angle of the light source was approximately 30°. The light source was approximately 20 cm away from the samples. The imaging spectrometer coupled with a microscope was placed immediately above the samples. The distance between the objective lens and the sample was adjusted so that the needle sample was clearly imaged in the scope of the imaging spectrometer. After adjustment, the light source, imaging spectrometer, and microscope were not changed in the whole measurement process. Since the light intensity of the artificial light source was stable, the standard reference panel was only measured at the beginning of the measurement.

Three, four, and three needle samples were taken from the top, middle, and lower layers of the larch tree (a total of ten needles), respectively. As in previous experiments, the samples were placed on a 100% cotton fabric in black during measurement, and was pinned to the black cloth with two small pushpins. Two images of the adaxial side were taken for each larch needle. One image was taken with the azimuth of the larch needle consistent with the azimuth of the light source (Fig. 4 (a), this placement manner is called parallel placement hereafter), and the other image was taken with the azimuth of the larch needle perpendicular to the azimuth of the light source (Fig. 4(b), this placement manner is called perpendicular placement hereafter). The projected interception area of light for the parallel placement is not the same as that for the perpendicular placement due to the three-dimensional structure of the needle.

Three needles were taken from each of the top, middle, and lower layers of a Scotch pine tree (a total of nine needles). Since the Scotch pine needle is relatively curved, it is difficult to control the azimuth. The morphological difference between the abaxial side and adaxial side of the Scotch pine needle is more obvious than the larch needle, so the Scotch pine needles were used to analyze the BRF difference between the adaxial and abaxial sides. Therefore, two images were also taken of each Scotch pine needle, one of which was the adaxial side of the needle and the other of which was the abaxial side of the needle. Eighteen hyperspectral images of Scotch pine needles were obtained.

In particular, the ten larch needles and nine Scotch pine needles were used to analyze the relationship between Cab and BRF. After the BRF of a needle was measured, the Cab of this needle was immediately measured with a CCM-300 instrument. For Scotch pine needles, the Cab of the adaxial and abaxial sides of nine needles was measured. The Cab of nine larch needles was measured because one larch needle was yellow. The larch needles were mainly used to analyze the effect of the needle azimuth on the relationship between BRF and Cab. Therefore, only the single-side (adaxial) Cab of the larch needles was measured.

2.3.5. Calculation of needle BRF and vegetation indices

Hyperspectral images recorded the DN values of 128 bands from 400 nm to 1000 nm. Even with the magnification of the microscope, the strips and natural needles did not cover the whole field of view (FOV) of SOC710-VP, indicating that there was part of the black cloth in the images of needle samples. To obtain the BRF of the samples, a reasonable DN threshold value was set according to the light intensity during imaging to distinguish sample pixels from black cloth pixels. The threshold was set to 30% of the DN value of the incident light at 752 nm (DN_r/R_r in Eq. (3)), higher than the pixel values of the black cloth. The 75th band

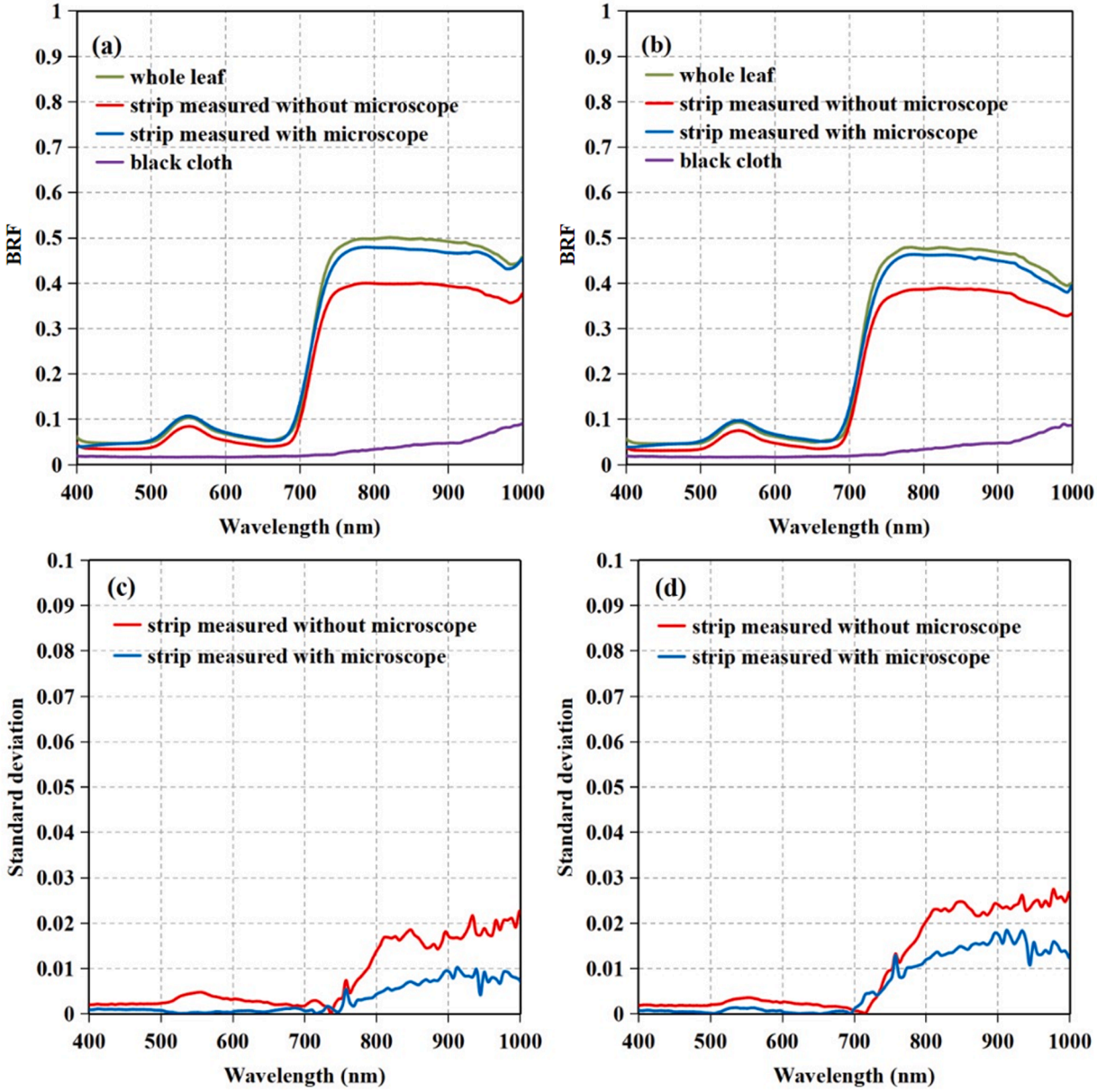

Fig. 5. BRF spectra and standard deviations of the spectra of the two replicates of samples. Each replicate included three quasi-needle samples of a sycamore leaf. The green and purple curves in (a) and (b) represent the BRF curves of the intact leaf and black cloth, respectively. The red curves represent the mean BRF (in (a) and (b)) or the standard deviations of the spectra (in (a) and (b)) of three narrow strips measured without the microscope. The blue curves represent the mean BRF (in (a) and (b)) or the standard deviations of the spectra (in (a) and (b)) of three narrow strips measured with the microscope.

(752 nm) was used in this study because the needle samples have much higher BRF in this band, which can achieve a better distinction between samples and background. Second, the normalized difference vegetation index (NDVI) of each pixel was calculated (669 nm for the red band and 779 nm for the NIR band), and a reasonable threshold of the NDVI was set to distinguish normal needle pixels from abnormal needle pixels. Abnormal needle pixels refer to needle pixels with obvious lesions and those with specular reflection. The NDVI of abnormal needle pixels was even lower than 0. The NDVI threshold set in this study was 0.3. Third, the extracted normal needle pixels and the corresponding reference panel pixels were used to calculate BRF with Eq. (3).

$$R_s = DN_s/(DN_r / R_r) \quad (3)$$

where R_s and R_r represent the BRF of the sample (*i.e.*, the whole sycamore leaf, the narrow strip, or the natural needle) and the standard reference panel, respectively. DN_s and DN_r refer to the averaged DN of a sample and that of the reference panel, respectively. The DN value of the incident light was obtained by dividing the measured DN value of the standard reference panel by the BRF of the standard reference panel (*i.e.*, DN_r/R_r).

Many vegetation indices (VIs) have been found to have good correlations with Cab at the leaf scale (Gitelson and Merzlyak 1994; Gitelson et al., 2003; Gitelson et al., 2006; Schlemmer et al., 2013) and at the canopy scale (Clevers and Gitelson 2013; Clevers and Kooistra 2011; Gitelson et al., 2005; Schlemmer et al., 2013). All of them were the ratios or differences based on two or three spectral bands located in the spectral domain from 450 nm to 850 nm. In this study, two simple and widely used VIs, *i.e.*, the red-edge simple ratio ($SR_{red\text{-}edge}$) and the modified normalized difference ($NDVI_m$), were calculated from the measured BRF to analyze the correlations between these two VIs and Cab, respectively. The $SR_{red\text{-}edge}$ was the ratio of the BRF at 750 nm to the BRF at 705 nm ($\frac{R_{750}}{R_{705}}$, where R refers to the BRF) (Gitelson and

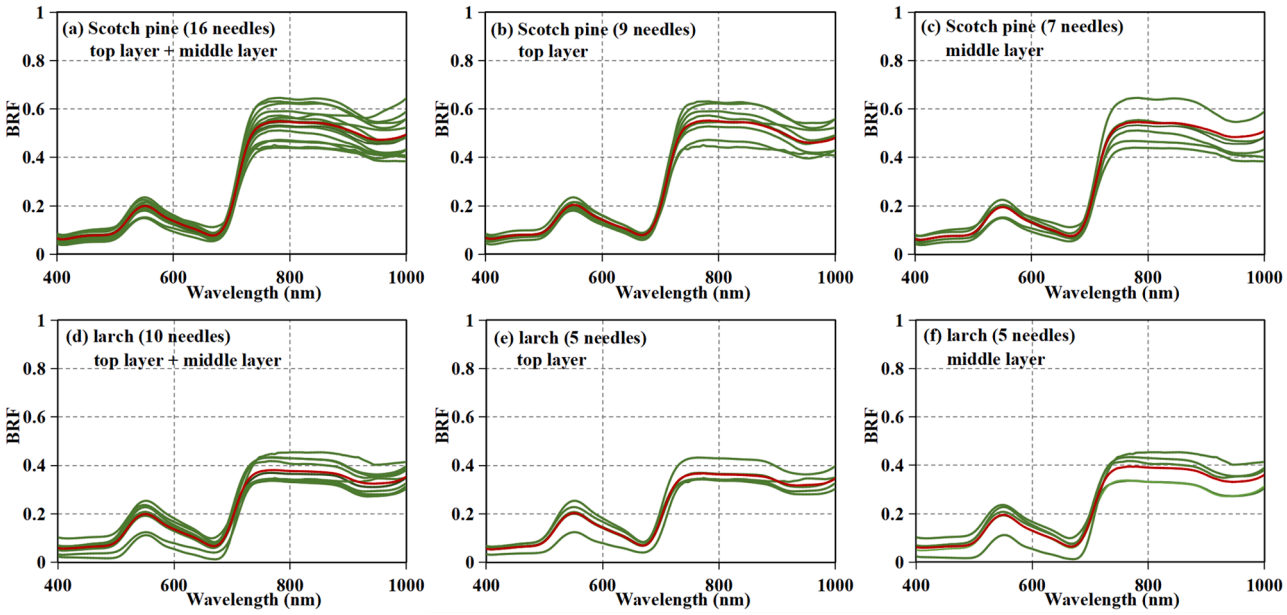

Fig. 6. The BRF of natural samples measured under natural light is shown. The curves in (a) and (d) are the BRF curves of all needles of Scotch pine and larch, respectively. The curves in (b), (c), (e), and (f) are the BRF curves of needles plucked from the top and middle parts of the canopies of Scotch pine and larch, respectively. The bold red curves from (a) to (f) are the mean BRF curves.

Merzlyak 1994). The $NDVI_m$ was calculated as the normalized difference between the BRF at 750 nm and that at 705 nm ($\frac{R_{750}-R_{705}}{R_{750}+R_{705}}$) (Gitelson and Merzlyak 1994). Due to the spectral resolution of the SOC710-VP imaging spectrometer (4.69 nm), the BRF at 752 nm and 705 nm was used to calculate the two VIs instead.

3. Results and discussion

3.1. Measurement results of narrow strips of broad leaves

The measurement results of the two replicates of samples, *i.e.*, BRF spectra and standard deviations of the BRF of narrow strips, are shown in Fig. 5. The BRF of the narrow strips (red and blue curves in Figs. 5(a) and (b)) was the average BRF of the three strips from the same sycamore leaf. The BRF reached a maximum at approximately 750 nm, which was mainly caused by the scattering properties of leaves (Gitelson and Merzlyak 1994). The BRF curves of each replicate showed the same characteristics, *i.e.*, the BRF peak of the green band (approximately 550 nm), the BRF valley of the red band (approximately 690 nm), and the continuous near-infrared BRF plateau.

However, there were differences between the green, red, and blue curves in Figs. 5(a) and (b). The BRF of narrow strips measured without the microscope (red curves in Figs. 5(a) and (b)) was seriously lower than that of the whole sycamore leaf (green curves in Figs. 5(a) and (b)) for each band. The mean differences in BRF at 400–700 nm (visible bands) and 700–1000 nm (near-infrared bands) were 0.015 and 0.090, respectively. The narrow strips were approximately 2 mm wide, corresponding to only approximately 6 pixels on the images measured without the microscope. It was difficult to extract pure strip pixels (uncontaminated by the background) from the images and the number of extracted needle pixels was limited. Therefore, the BRF of strips measured without a microscope was much lower than the BRF of whole sycamore leaves, especially for the near-infrared bands. In contrast, the BRF curves of the strips measured with a microscope (blue curves in Figs. 5(a) and (b)) were basically consistent with the BRF curves of the whole leaf (green curves in Figs. 5(a) and (b)). The mean differences in BRF at 400–700 nm (visible bands) and 700–1000 nm (near-infrared bands) were 0.0043 and 0.019, respectively. The standard deviations of the BRF of narrow strips were also lower than those measured without a microscope. After being magnified by the microscope, the strip was more than 80 pixels wide on the image; therefore, it was easy to extract pure strip pixels from the images. The BRF of the strips measured with a microscope was still slightly lower than that of the whole sycamore leaves in near-infrared bands, which may have been caused by part of the light inside the strips scattered from the sides of the strips (Zhang et al., 2008). The width of some types of conifer needles was less than 2 mm (*e.g.*, larch). Therefore, it was necessary to use a microscope coupled with an imaging spectrometer to measure the spectrum of conifer needles.

3.2. Measurement results of conifer needles under natural light

The BRF results of Scotch pine and larch needles measured under natural light, are shown in Fig. 6. The mean proportions of normal pixels were 54% and 66% for the Scotch pine and larch needles, respectively. The measured BRF of needle samples exhibited the same characteristics as the BRF of sycamore leaves. However, needle samples had higher BRF in the green band (approximately 550 nm; Fig. 6) than sycamore leaves (Fig. 5). There were large differences between the BRF of the two different coniferous species and large intraclass differences among the BRF of each conifer species (Figs. 6(a) and (d)). The average standard deviations of the BRF of Scotch pine needles for visible (400–700 nm) and near-infrared regions (700–1000 nm) were 0.016 and 0.058, respectively, while those of larch needles for visible and near-infrared regions were 0.031 and 0.043, respectively. Intraclass differences may be due to the measured needles being at different age cohorts, or growing in different vertical layers with different direct/diffuse radiation conditions (Hovi et al., 2017; Lhotáková et al., 2007; Lukeš et al., 2013; O'neill et al., 2002). The average BRF of the Scotch pine needles (bold red curve in Fig. 6(a)) was higher than that of larch needles (bold red curve in Fig. 6(d)), especially for the near-infrared bands. The average BRF of needles in the top layer was close to that in the middle layer for the same species (bold red curves in Fig. 6(b), (c), (e), and (f)). The measured Cab had the same characteristics. The average Cab of needles in different layers of Scotch pine was close to each other (63.27 $\mu g \cdot cm^{-2}$ for the top layer and 63.85 $\mu g \cdot cm^{-2}$ for the middle layer), as was larch (23.74 $\mu g \cdot cm^{-2}$ for the top layer and 25.51 $\mu g \cdot cm^{-2}$ for the middle layer).

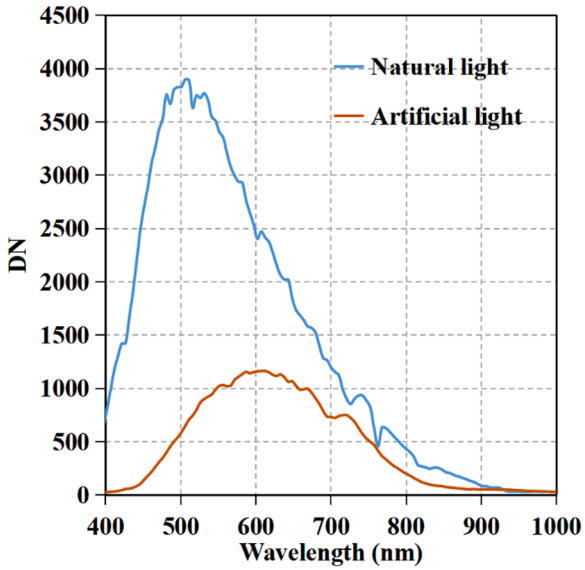

Fig. 7. The DN value curves of natural light (blue curve) and artificial light (red curve). The DN values of natural light and artificial light were obtained by dividing the measured DN value of the standard reference panel by the BRF of the standard reference panel (50%).

3.3. Measurement results of conifer needles under artificial light

3.3.1. Comparison of natural light and artificial light

The DN value of incident light was obtained by dividing the measured DN value of the standard reference panel by the BRF of the standard reference panel. The DN values of natural light and artificial light measured by a SOC710-VP imaging spectrometer coupled with a microscope are shown in Fig. 7. The integration time of SOC710-VP was the same, *i.e.*, 99.82 ms (the maximum value of the instrument), when measuring the DN value of natural light and artificial light. The DN value of natural light is basically greater than that of artificial light in a wavelength range from 400 nm to 1000 nm. When the wavelength was less than 450 nm and more than 850 nm, the DN value of artificial light was less than 100, and the DN value of the black cloth was approximately 7. To ensure a large signal-to-noise ratio, *i.e.*, the ratio of the DN value of artificial light to the DN value of black cloth greater than 15, only the BRF in a wavelength range of 450 nm to 850 nm was calculated. Therefore, the wavelengths below 450 nm and above 850 nm were excluded when analyzing the measurements made under the artificial light in September.

3.3.2. Adaxial and abaxial sides of the conifer needle

The BRF curves of the adaxial and abaxial sides of Scotch pine needles are shown in Fig. 8. The mean proportions of normal pixels were 38% and 48% for the adaxial and abaxial sides of Scotch pine needles, respectively. According to the measurement results, the BRF of the adaxial and abaxial sides of the same needle was different, *e.g.*, the BRF of the adaxial side in near-infrared bands was higher than that of the

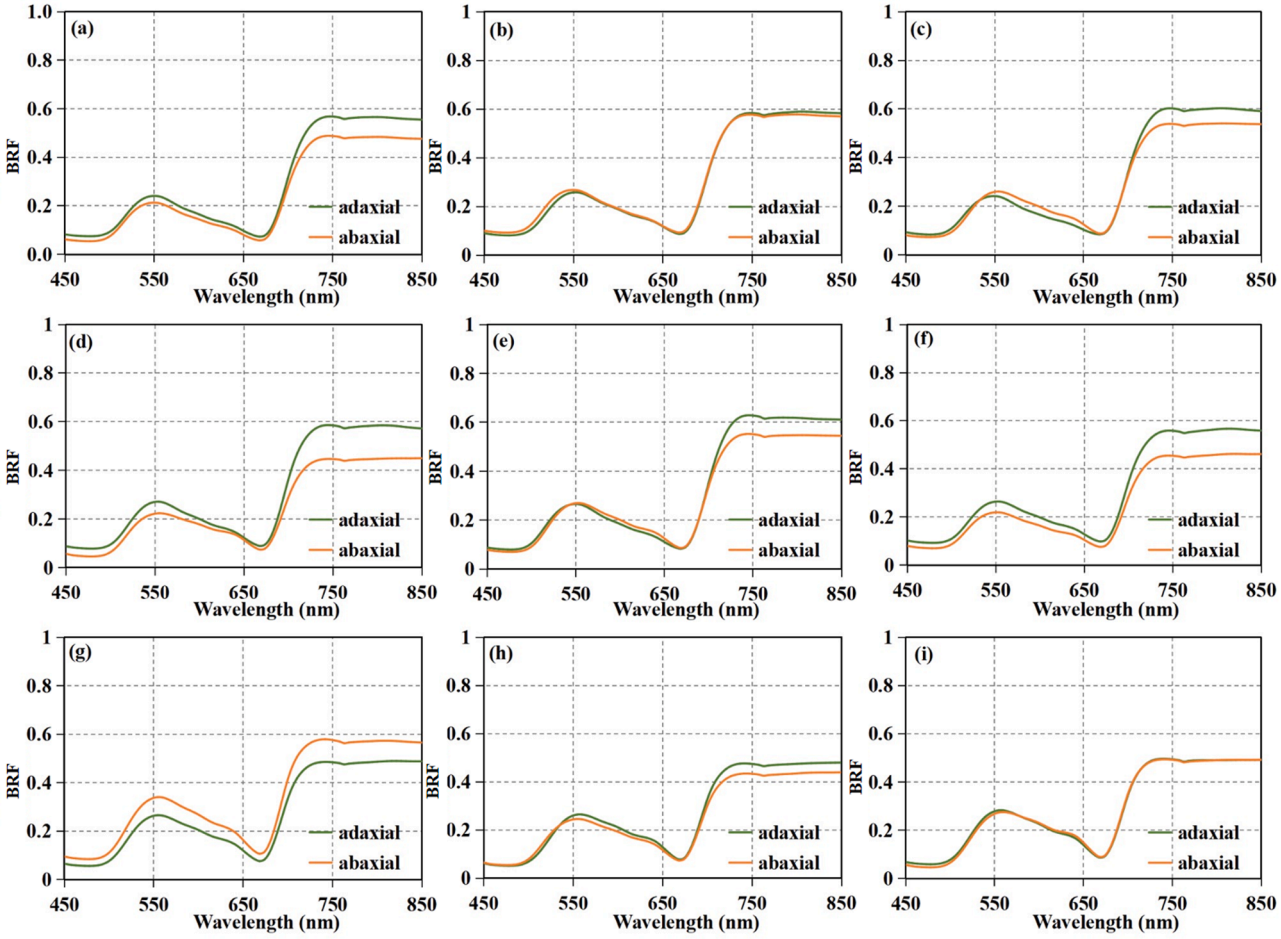

Fig. 8. Diagrams (a) - (i) are the BRF curves of nine Scotch pine needles measured under artificial light. The yellow curves and green curves in the diagrams are the BRF curves of the abaxial sides and adaxial sides of the Scotch pine needles, respectively.

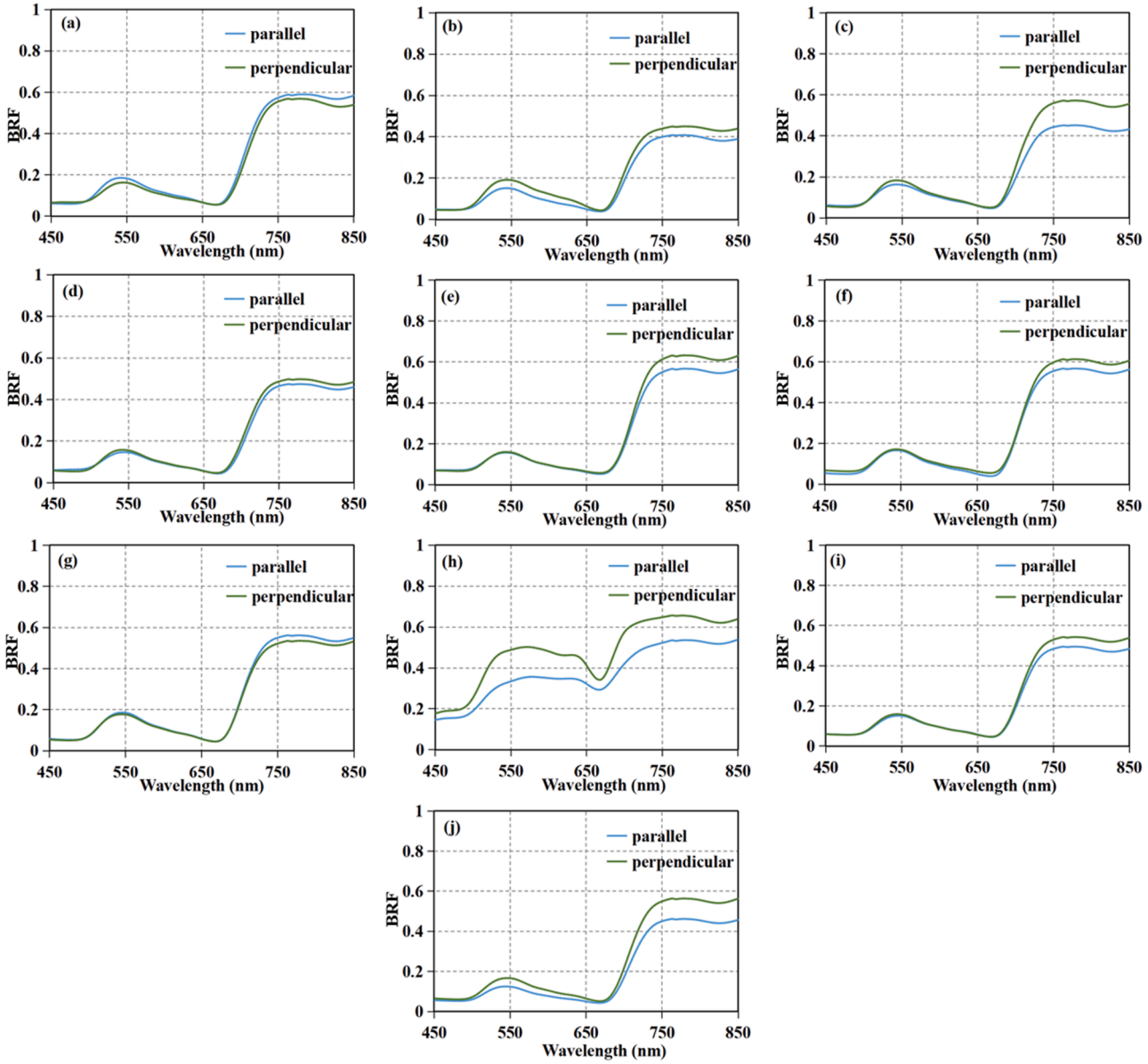

Fig. 9. Diagrams (a) - (j) are the BRF curves of ten larch needles measured under artificial light. The green and blue curves in the diagrams are the BRF curves measured at the azimuths of larch needles perpendicular and parallel to the solar azimuth, respectively.

abaxial side, except for one needle (Fig. 8(g)). The differences between the BRF of the two leaf sides were shown in other studies (de Marín et al. 2016; Middleton et al., 1997). The differences in BRF may be caused by the bidirectional reflectance distribution function (BRDF) effects since the adaxial side of the Scotch pine is flat while the abaxial side is rounded. For coniferous species with bifacial and non-flat leaves, it is vital to obtain the BRF of both sides of bifacial leaves to understand reflectance characteristics at the canopy level (Rautiainen et al., 2018).

3.3.3. *Different azimuths of conifer needle*

The BRF of larch needles measured in the perpendicular placement and in the parallel placement is shown in Fig. 9. The mean proportions of normal pixels were 76% and 88% for the larch needles measured in the perpendicular placement and in the parallel placement, respectively. Except for two needles (Figs. 9(a) and (g)), the needle BRF values measured in the perpendicular placement (Fig. 4(b); green curves in Fig. 9) were higher than that measured in the parallel placement (Fig. 4 (a); blue curves in Fig. 9), especially for the near-infrared bands. The measured BRF curve of a yellow needle (Fig. 9(h)) was considerably different from that of the other needle samples. When the needles were placed at different azimuths, the angles between the incident light and the needle were different, which resulted in different projected interception areas of light and BRDF effects. This may explain the differences in BRF between the two placement methods. Compared to the broadleaf that can be regarded as a plane, the structure of conifer needles are more complex, which makes the scattering of light more complex and the BRF of needles considerably affected by the azimuth of the needle (the maximum difference between BRF at two azimuths in the near-infrared bands was 0.125 in Fig. 9(c)).

3.4. *The relationship between chlorophyll content and vegetation indices*

The results of the experiment conducted under artificial light are presented here. The Cab of the adaxial side of Scotch pine needles obtained from the top and middle layers of the canopy was higher than that of larch needles (Figs. 10(a) and (b)). Furthermore, as illustrated in Figs. 10(b) and (c), the Cab of the adaxial side of Scotch pine leaves obtained from the top and middle layers of the canopy was higher than

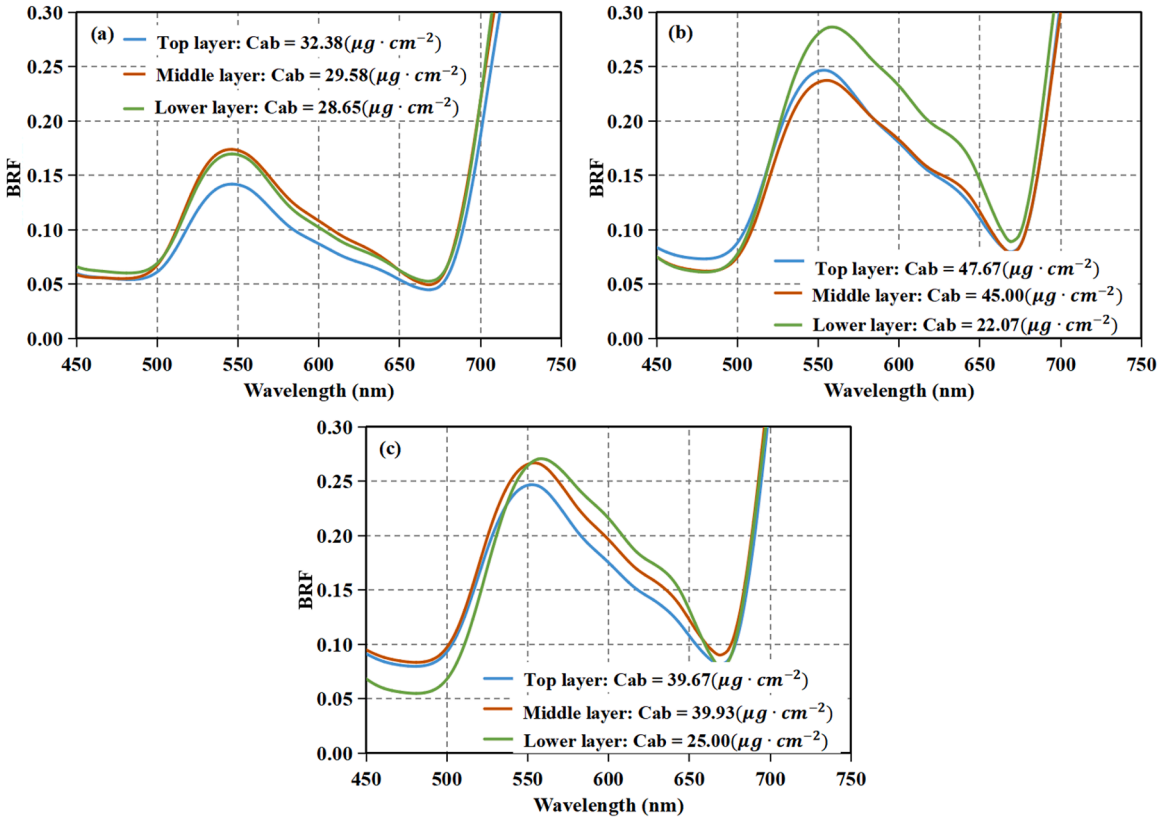

Fig. 10. The average BRF and average chlorophyll content (Cab) of three vertical canopy layers in the experiment conducted under artificial light. (a), (b), and (c) are the BRF spectra of the adaxial side of larch needles, the adaxial side of Scotch pine needles, and the abaxial side of Scotch pine needles, respectively.

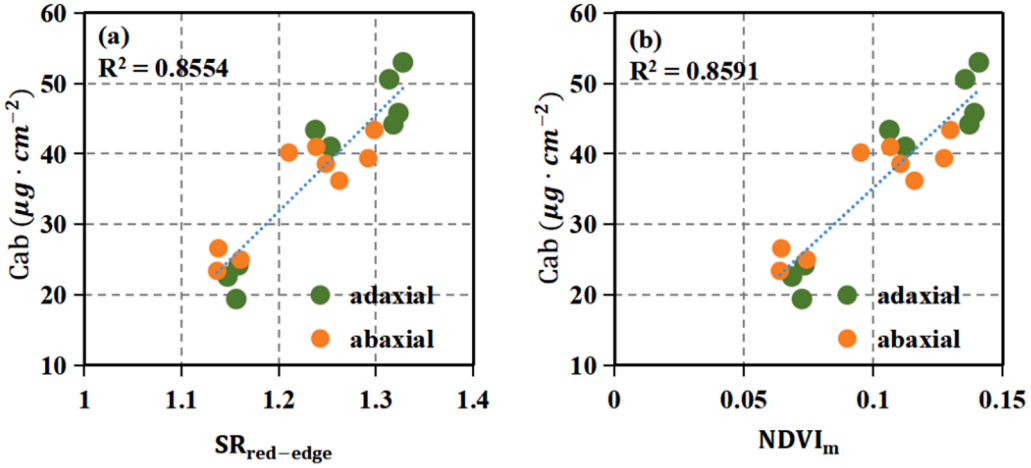

Fig. 11. The relationship between two vegetation indices ((a) $SR_{red\text{-}edge}$ and (b) $NDVI_m$) and chlorophyll content (Cab) of Scotch pine needles.

that of the abaxial side of the same leaves. For the same conifer species, the difference between the Cab of the three vertical layers led to a difference in needle BRF in the following two aspects. First, when the Cab was high, the BRF in the visible region was low, especially for the green band (approximately 550 nm). Second, when the Cab was high, the red edge moved towards long wavelengths. These phenomena have been found in other studies (Daughtry et al., 2000). Cab drives most leaf BRF variabilities in the visible domain (Jay et al., 2017). The BRF of the blue and red bands was not sensitive to the change in Cab, which may be caused by the saturation effect (Daughtry et al., 2000) (due to the strong absorption of Cab). Gitelson and Merzlyak (1994) also found that the BRF changes in the blue (400–500 nm) and red (near 670 nm) bands were smaller than those in the green band (near 555 nm).

The relationships between the two VIs (*i.e.*, $SR_{red\text{-}edge}$ and $NDVI_m$) and Cab of Scotch pine needles are presented in Figs. 11(a) and (b). According to Fig. 11, both VIs had good linear relationships with Cab. The coefficients of determination (R^2) for $SR_{red\text{-}edge}$ (Fig. 11(a)) and $NDVI_m$ (Fig. 11(b)) were 0.8554 and 0.8591, respectively. Other studies also showed that the two indices had good linear relationships with leaf Cab (Gitelson and Merzlyak 1994).

The relationships between the two VIs calculated by the BRF measured in different placement methods of needle azimuth and the Cab of larch needles are shown in Fig. 12. According to the R^2 value, the linear relationship of VIs and Cab with the perpendicular placement of

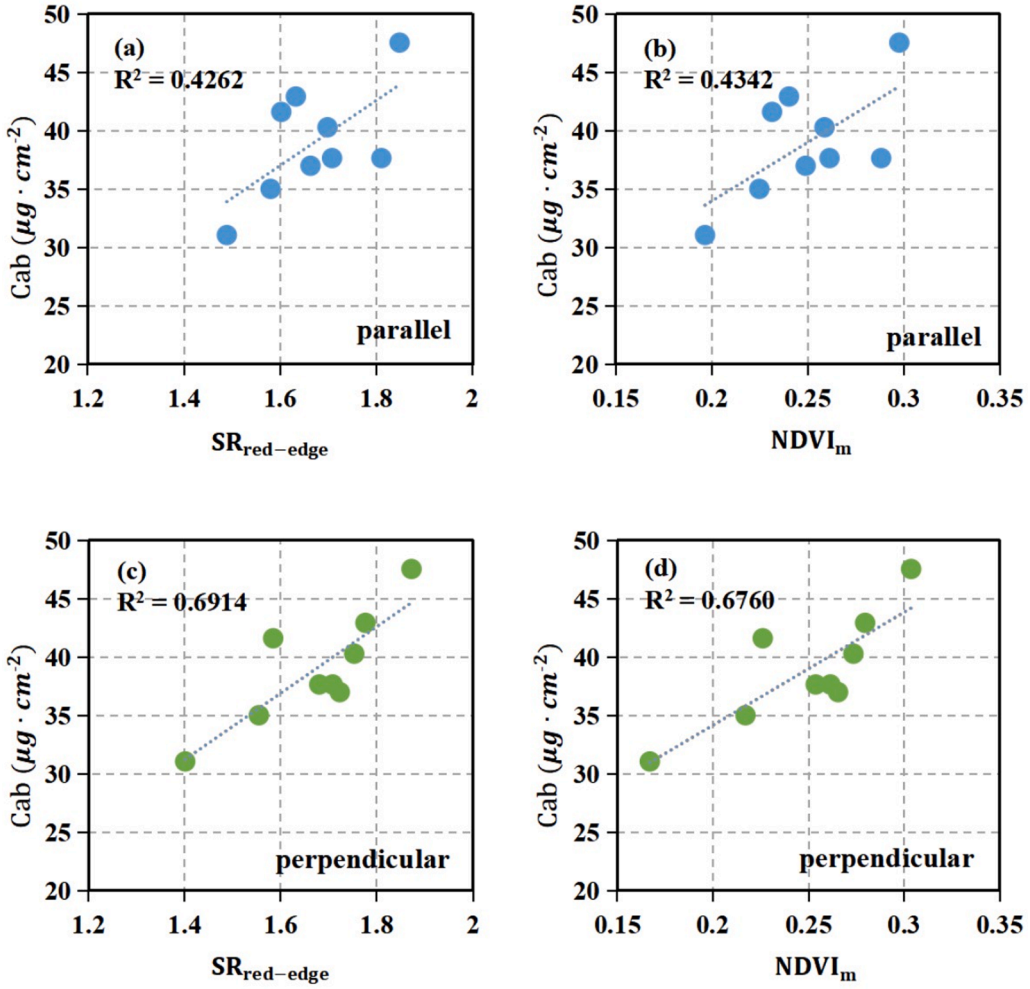

Fig. 12. The relationships between two vegetation indexes and chlorophyll content (Cab) of larch needles. (a) and (b) are the results measured with the needle azimuth parallel to the solar azimuth, while (c) and (d) are the results measured with the needle azimuth perpendicular to the solar azimuth.

needle azimuth was better than that with the parallel placement of the needle azimuth. A larger interception area of light for the perpendicular placement than the parallel placement corresponded to more radiation transferred from the tissues within a needle and higher BRF in the near-infrared bands (Fig. 9). This indicated that when measuring needle BRF, the placement of needle azimuth relative to the sun-observer geometry could affect the correlation between Cab and VIs calculated from the measured BRF.

3.5. *The analysis of influential factors for microscopy imaging method*

3.5.1. *The influence of specular reflection*

Specular reflection on the surface of needles, observed in hyperspectral images taken under natural and artificial light, was related to needle shape and waxy cuticle. Specular reflection appeared as bright spots in the true-color images synthesized by red, green, and blue bands (Fig. 1). When the radiation reached the leaf surface, one part passed through the leaf surface and the other part was reflected back to the atmosphere by the waxy cuticle (Grant 1987). The radiation reflected by the leaf surface did not interact with leaf pigments and internal leaf structures (Grant 1987). Specular reflection occurred on the leaf surface and seriously increased the radiation directly reflected by the leaf surface.

The experiments this far always removed the specular reflection (*i.e.*, all results shown until now were without specular reflection). The BRF with specular reflection effects in this section was obtained without setting the NDVI threshold (*i.e.*, the second step in Section 2.3.5 was not performed) in the experiment made under artificial light in September. The BRF calculated with specular reflection and the BRF calculated without reflection were hereafter called R_p and R_{np}, respectively. The R_p of the two sides of Scotch pine needles was higher than R_{np} of the two sides of Scotch pine needles (Figs. 13(a) and (b)). Similarly, the R_p of the adaxial side of larch needles measured at different azimuths was higher than R_{np} of the adaxial side of larch needles measured at different azimuths (Figs. 13(a) and (b)). Additionally, the linear correlation between Cab and $SR_{red\text{-}edge}$ calculated by R_p (Figs. 13(c), (d) and (e)) was worse than that between Cab and $SR_{red\text{-}edge}$ calculated by R_{np} (Figs. 11(a), 12 (a) and (c)).

The characteristics of the leaf BRF spectrum are the result of the interaction of various pigments and complex structures in leaves. Since specular reflection affects the correlation between needle BRF and Cab, it is necessary to exclude the influence of specular reflection from BRF calculations. By setting the NDVI threshold, it is easy to remove the specular reflection from the hyperspectral images of needles.

The measured needle BRF can be used not only to retrieve the Cab but also to serve as a basic parameter to establish and verify the canopy radiative transfer model. The reflection properties of needles are very complex, and few models consider the specular reflection of needles. Our measurements can help advance this aspect of the modeling effort.

3.5.2. *The effect of DN threshold and NDVI threshold on BRF measurement*

The DN threshold and NDVI threshold are needed to extract normal

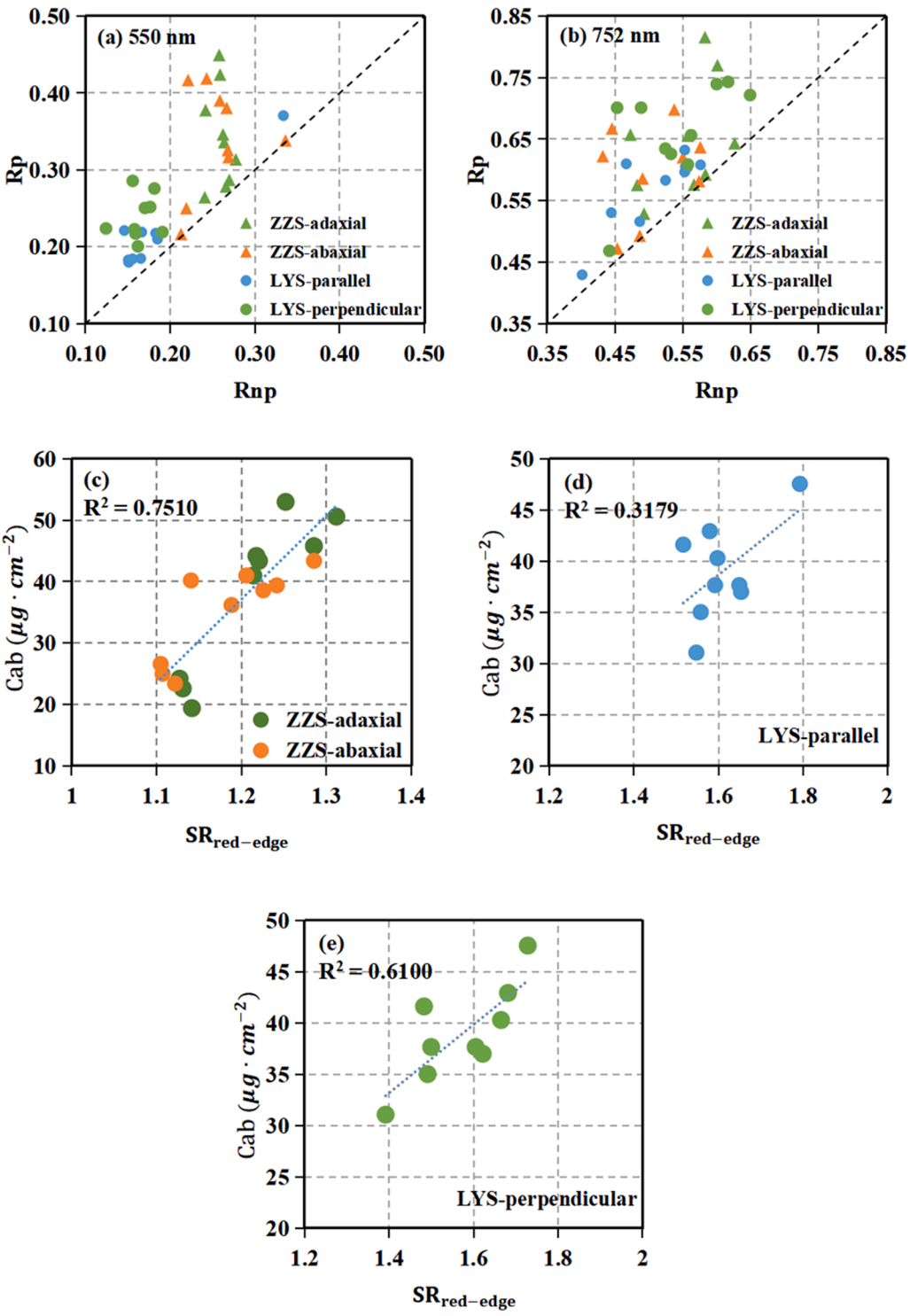

Fig. 13. Influence of specular reflection on the measurement of needle BRF. ZZS and LYS respectively represent the Scotch pine and the larch. (a) and (b) are the scatter plots of BRF of the adaxial and abaxial sides of nine Scotch pine needles and of the adaxial sides of ten larch needles with (R_p) and without specular reflection (R_{np}) at 550 nm and 752 nm, respectively. The BRF of Scotch pine needles was measured with the needle azimuth perpendicular to the light azimuth, while the BRF of larch needles was measured with needle azimuth perpendicular or parallel to the light azimuth. (c), (d), and (e) show the relationships between $SR_{red\text{-}edge}$ and chlorophyll content (Cab) of needles. $SR_{red\text{-}edge}$ is the BRF ratio of needles at 752 nm and 705 nm. The $SR_{red\text{-}edge}$ of (c),(d), and (e) are calculated using R_p.

needle pixels from hyperspectral images (Section 2.3.5). The DN threshold was set to 30% of the DN value of the incident light at 752 nm (hereafter called the $DN_{30\%}$) to distinguish the needles from the background of low BRF. The NDVI threshold was set to 0.3 to distinguish normal needle pixels from abnormal needle pixels. To analyze the sensitivity of the microscopy imaging method to those two thresholds, the DN thresholds were respectively set to 10%, 20%, and 40% of the DN value of the incident light at 752 nm (hereafter called the $DN_{10\%}$, $DN_{20\%}$, and $DN_{40\%}$, respectively), and the NDVI thresholds were respectively set to 0.2 and 0.4 to recalculate the BRF of needles. When analyzing the effect of DN thresholds, the NDVI threshold was fixed and set to 0.3. Since the larch needles and Scotch pine needles showed the similar characteristics of BRF, only the measurement results of the abaxial side of the nine Scotch pine needles under artificial light were shown below for the brevity.

The measurement results for different DN thresholds are presented in Fig. 14. The calculated BRF of the nine needles showed similar variation characteristics when the DN threshold was changed, *i.e.*, the measured BRF decreased as the DN threshold decreased. However, the BRF changes of the nine needles were different in magnitude. The BRF at 752

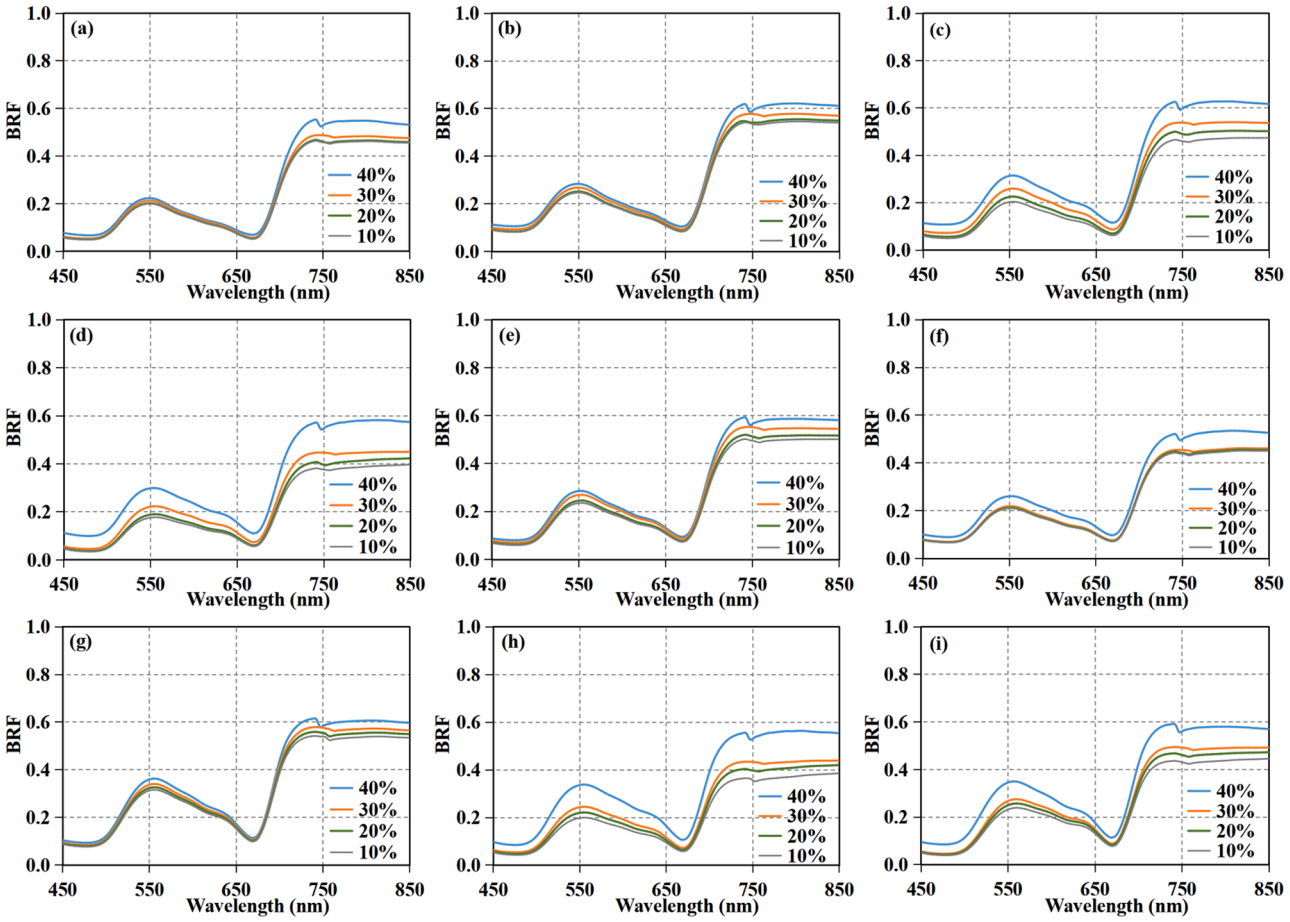

Fig. 14. Influence of DN threshold on the measurement of needle BRF. (a) - (i) are the measured BRF of the abaxial sides of nine Scotch pine needles with four different DN thresholds, respectively. 40%, 30%, 20% and 10% means that the DN thresholds were set to 40%, 30%, 20% and 10% of the DN value of the incident light at 752 nm, respectively.

nm was changed by at most 0.185 (Fig. 14(h)) and by at least 0.050 (Fig. 14(g)) when the DN threshold was changed from $DN_{10\%}$ to $DN_{40\%}$. Although the needle images were magnified with a microscope, there were still mixed pixels in the hyperspectral images, such as those pixels at the edges of the needles. Using a lower DN threshold resulted in more mixed needle pixels in the calculation of needle BRF. Therefore, the BRF calculated with $DN_{10\%}$ was lower than those with the other two DN thresholds. A DN threshold high enough should be selected to eliminate the influence of the background. Generally, needle BRF in the near-infrared band is higher than 0.3, while the BRF of black cloth in the near-infrared band is less than 0.09. However, using a threshold that is too high could cause a proportion of needle pixels to be identified as background pixels. The mean proportion of normal needle pixels for $DN_{40\%}$ was only 22%, while that for $DN_{30\%}$ was 48%. Thus, the $DN_{30\%}$ is recommended to reduce the number of mixed pixels and obtain accurate BRF.

The results for a fixed DN threshold ($DN_{30\%}$) and three different NDVI thresholds are shown in Fig. 15. The measured BRF of the nine needles increased with the decrease of the NDVI threshold. The BRF at 752 nm was changed by at most 0.12 (Fig. 15(c)) and by at least 0.0027 (Fig. 15(a)). The NDVI of abnormal needle pixels with high BRF was even lower than 0. Using a low NDVI threshold resulted in more abnormal needle pixels in the selected normal needle pixels. However, using a high NDVI threshold caused a proportion of normal needle pixels to be identified as abnormal pixels. A moderate NDVI threshold, *e.g.*, 0.3, may be suitable to select normal needle pixels.

3.6. The advances and limitations

The traditional method uses nonimaging spectrometers to measure the directional-hemispherical reflectance factor (DHRF) of needles. The nonimaging spectrometer records the mixed signals of various substances in the FOV of the sensor. To obtain the RF of needle, the first method is to fill the FOV with needles, the second method needs to calculate the area occupied by gaps in the FOV, and the third method requires removing the spectral contribution of the sample holder. These methods can only measure the RF of multiple needles at the same time, but cannot measure the RF of a single needle. Long and thin needles placed together can lead to multiple scattering (Daughtry et al., 1989; Yanez-Rausell et al., 2014b), in which adjacent needles lead to the measured RF being higher than the actual value, especially in the near-infrared bands. Although in the second method, the effect of multiple scattering can be reduced when the distance between adjacent needles is greater than 0.5 times the needle width (Yanez-Rausell et al., 2014a), the uncertainty of measured RF is dependent on the gap fraction (Ramsey and Rangoonwala 2004). The larger the gap fraction, the smaller the signal from the needles, and thus smaller signal to noise ratio. The third method is marginally affected by multiple scattering since each needle is located in a slot individually. However, due to the different shapes of needles, it is difficult to make a fully suitable slot in actual measurements, which may lead to light leakage and inaccurate measurements.

In contrast, the imaging spectrometer can directly measure the BRF of a single needle without measuring other variables (*e.g.*, gap fraction) with the help of the magnification function of the microscope. Since

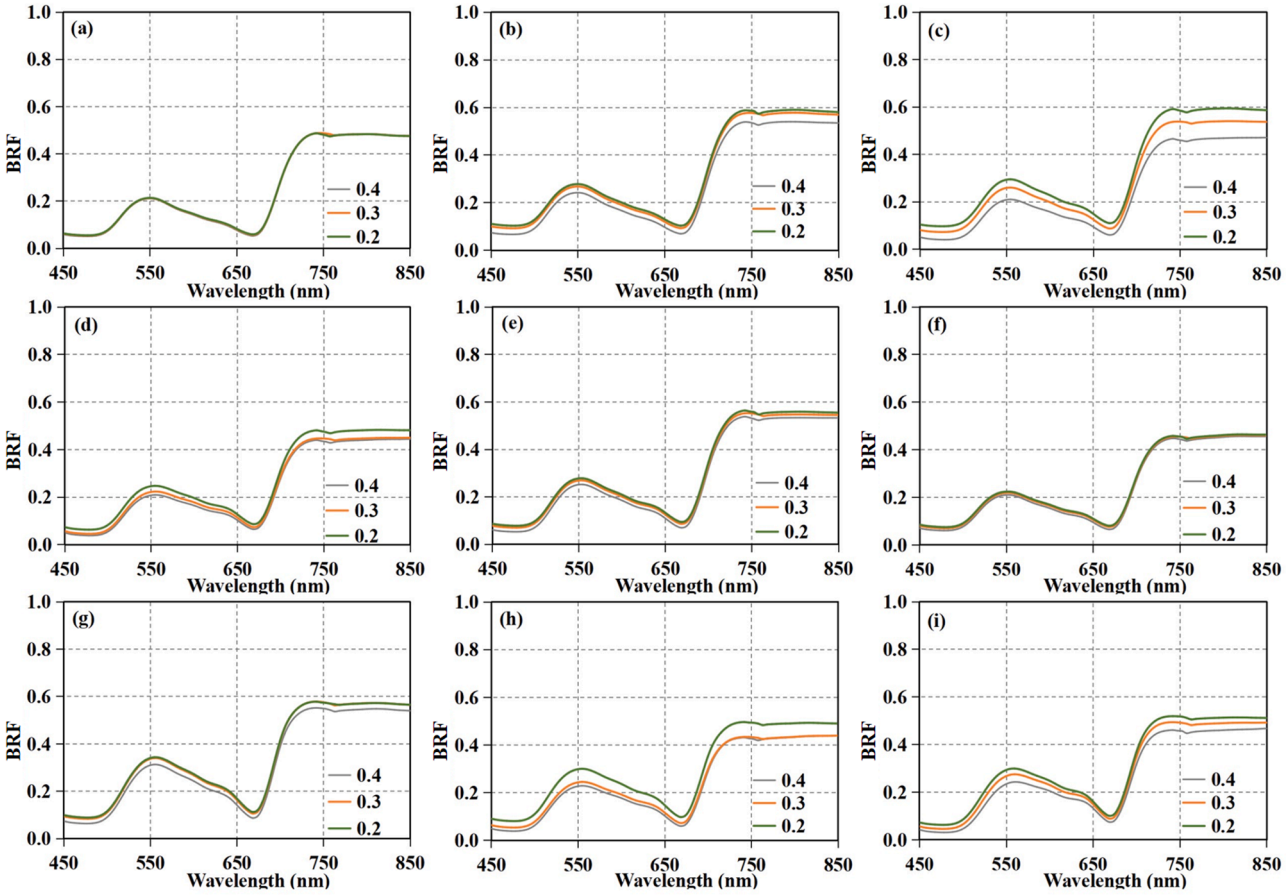

Fig. 15. Influence of the threshold of excluding abnormal needle pixels on the measurement of needle BRF. (a) - (i) are the measured BRF of the abaxial side of nine Scotch pine needles with three different NDVI thresholds (*i.e.*, 0.4, 0.3 and 0.2), respectively.

pure needle pixels can be extracted from hyperspectral images after microscope magnification, the microscopy imaging method could provide precise results. Thus, this method has the potential to be used to establish a spectral database of BRF for needles.

The quantities measured by the traditional methods and by the microscopy imaging method have different physical meanings. The DHRF measured by the traditional methods is an average of the BRF in each view direction in the hemispherical space, and is typically the input variable of one-dimensional canopy radiative transfer model, *e.g.*, the scattering by arbitrary inclined leaves (SAIL) model, which assumes that leaves are perfect Lambertian diffusors (Verhoef 1984). Due to the complex shape of needles, the anisotropy of needle BRF could be more prominent than that of broad leaves. To better understand the radiative transfer process and establish accurate radiative transfer models at canopy and leaf scales, it is necessary to measure the BRF of needles (Bousquet et al., 2005). For example, Shi and Xiao (2021) developed a canopy-scale radiative transfer model considering leaf dorsoventrality. Three-dimensional canopy radiative transfer models may consider foliage properties in more details and require the BRF as an important input parameter. The microscopy imaging method offers the possibility of measuring the BRF of the needle. However, estimating the DHRF and the entire BRDF (*i.e.*, making measurements from different view directions) of needles with the microscopy imaging method would be slow since measurements at multiple view angles are needed. For simple measurements of absorption or hemispherical reflectance/transmittance factor, the traditional method is probably easier and faster. Thus, it is expected that the synergies between the microscopy imaging method and traditional methods contribute to better understanding of the spectral scattering and absorption properties.

The microscopy imaging method was not used to measure the transmittance of needles in this study, but this could be achieved by shine the artificial light upward from under the sample. Although the so-called transmittance of needles can be measured, how to define this term needs to be discussed. Wang et al. (2020) claimed that the reflected and transmitted radiation of a needle should be distinguished by the illuminated and shaded surfaces. They analyzed the possible problems of traditional methods (Wang et al., 2020). Since the needles of many conifer species lack a flat surface required by the definition of reflectance and transmittance, Rautiainen et al. (2018) believed that it is more justified to interpret reflectance and transmittance as backward and forward scattering, respectively. In addition, it should be noted that if the microscopy imaging method is used to calculate the absorption of needles (*i.e.*, incidence minus reflection and transmission), the specular reflection should be included in the calculation of reflection.

Since the spectral region of SOC710-VP is from 400 nm to 1000 nm, only the BRF in this region can be measured. This spectral region is insufficient for some practical applications. Hyperspectral imagers for longer wavelengths, *e.g.*, SOC710-SWIR (Surface Optics Corporation, USA) with a spectral region from 900 nm to 1700 nm, will be necessary if the short-wave infrared spectrum is needed. Another possible solution is to first choose a suitable leaf-scale radiative transfer model, *e.g.*, the PROSPECT model (Jacquemoud and Baret 1990), and then invert the parameters of the model to simulate a full-range spectrum.

4. Conclusion

Since needle reflectance is indispensable in many remote sensing applications such as estimation of needle chlorophyll content (Cab), conifer species classification, and establishing canopy reflectance models for coniferous forests, accurate measurement of needle

reflectance is critical. The main difficulty is that conifer needle is too narrow to fully cover the field of view of the sensor (*e.g.*, spectrometer). Significant efforts have been made to solve this problem and three kinds of methods have been proposed. In this study, we proposed a new method to measure the bidirectional reflectance factor (BRF) of needles by integrating a hyperspectral imaging spectrometer and an optical microscope.

This method was used to measure the BRF of narrow strips of broad leaves and natural needle samples (larch and Scotch pine). The results show that the microscopy imaging method can accurately measure the BRF of thin and small leaves. The needle BRF of the adaxial side is generally higher than that of the abaxial side. The change in natural needle BRF measured by the microscopy imaging method is consistent with the change in natural needle Cab, *i.e.*, when the Cab is high, the needle BRF in the visible region is low. The vegetation indices (the red-edge simple ratio and modified normalized difference) calculated from the BRF at 705 nm and 752 nm have good linear relationships with the Cab. The measured BRF and the correlation between Cab and vegetation indices are affected by the needle azimuth (influence of up to 0.125 for the reflectance in near-infrared bands and 0.2 for R^2), indicating that a needle azimuth perpendicular to the solar azimuth is recommended in practice. In addition, with the help of the magnification function of the microscope, this method can be used to remove the specular reflection from the needle BRF and to promote the correlation between vegetation indices and Cab (an increase of R^2 values from 0.61 to 0.69 and from 0.75 to 0.85 for larch and Scotch pine, respectively). The microscopy imaging method is expected to optimize the needle BRF measurement to increase the understanding of reflected spectral signatures of conifers, and thus more efforts can be focused on the influence of the complex three-dimensional structures of the conifer needle (*e.g.*, uneven surface of needles) on the establishment of leaf-scale radiative transfer model with the help of micro vision.

Declaration of Competing Interest

The authors declare that they have no known competing financial interests or personal relationships that could have appeared to influence the work reported in this paper.

Data availability

Data will be made available on request.

Acknowledgments

This work is financially supported by the National Natural Science Foundation of China (Grant No. 42130104, 42090013, 42001271, and 42271338). This data set was provided by the Chengde Remote Sensing Test Site, State Key Laboratory of Remote Sensing Sciences. We sincerely thank the anonymous reviewers for comments that helped improve the quality of the manuscript.

References

Bousquet, L., Lachérade, S., Jacquemoud, S., Moya, I, 2005. Leaf BRDF measurements and model for specular and diffuse components differentiation. Remote Sens. Environ. 98, 201–211.
Carter, G.A., Paliwal, K., Pathre, U., Green, T.H., Mitchell, R.J., Gjerstad, D.H., 1989. Effect of competition and leaf age on visible and infrared reflectance in pine foliage. Plant Cell Environ.
Clevers, J.G., Gitelson, A.A., 2013. Remote estimation of crop and grass chlorophyll and nitrogen content using red-edge bands on Sentinel-2 and-3. Int. J. Appl. Earth Obs. Geoinf. 23, 344–351.
Clevers, J.G., Kooistra, L., 2011. Using hyperspectral remote sensing data for retrieving canopy chlorophyll and nitrogen content. IEEE J. Sel. Top. Appl. Earth Obs. Remote Sens. 5, 574–583.
Daughtry, C., Biehl, L.L. (1984). Changes in spectral properties of detached leaves.
Daughtry, C., B, L.L., R, K.J., 1989. A New Technique to Measure the Spectral Properties of Conifer Needles. Elsevier, p. 27.
Daughtry, C.S., Walthall, C., Kim, M., De Colstoun, E.B., McMurtrey Iii, J., 2000. Estimating corn leaf chlorophyll concentration from leaf and canopy reflectance. Remote Sens. Environ. 74, 229–239.
de Marín, S.T., Novák, M., Klančnik, K., Gaberščik, A., 2016. Spectral signatures of conifer needles mainly depend on their physical traits. Pol. J. Ecol. 64, 1–13.
Di Vittorio, A.V., 2009. Enhancing a leaf radiative transfer model to estimate concentrations and *in vivo* specific absorption coefficients of total carotenoids and chlorophylls a and b from single-needle reflectance and transmittance. Remote Sens. Environ. 113, 1948–1966.
Farjon, A., 2010. A Handbook of the World's Conifers (2 Vols. Brill.
Fourty, T., Baret, F., Jacquemoud, S., Schmuck, G., Verdebout, J., 1996. Leaf optical properties with explicit description of its biochemical composition: direct and inverse problems. Remote Sens. Environ. 56, 104–117.
Gates, D.M., Keegan, H.J., Schleter, J.C., Weidner, V.R., 1965. Spectral properties of plants. J. Ocul. Pharmacol. Ther. 4, 11–20.
Gausman, H.W., Allen, W.A., Cardenas, R., Richardson, A.J., 1970. Relation of light reflectance to histological and physical evaluations of cotton leaf maturity. J. Ocul. Pharmacol. Ther. 9, 545.
Gitelson, A., Merzlyak, M.N., 1994. Spectral reflectance changes associated with autumn senescence of Aesculus hippocastanum L. and Acer platanoides L. leaves. Spectral features and relation to chlorophyll estimation. Plant Physiol. 143, 286–292.
Gitelson, A.A., Buschmann, C., Lichtenthaler, H.K., 1999. The chlorophyll fluorescence ratio F735/F700 as an accurate measure of the chlorophyll content in plants. Remote Sens. Environ. 69, 296–302.
Gitelson, A.A., Gritz, Y., Merzlyak, M.N., 2003. Relationships between leaf chlorophyll content and spectral reflectance and algorithms for non-destructive chlorophyll assessment in higher plant leaves. Plant Physiol. 160, 271–282.
Gitelson, A.A., Keydan, G.P., Merzlyak, M.N., 2006. Three-band model for noninvasive estimation of chlorophyll, carotenoids, and anthocyanin contents in higher plant leaves. Geophys. Res. Lett. 33.
Gitelson, A.A., Vina, A., Ciganda, V., Rundquist, D.C., Arkebauer, T.J., 2005. Remote estimation of canopy chlorophyll content in crops. Geophys. Res. Lett. 32.
Grant, L., 1987. Diffuse and specular characteristics of leaf reflectance. Remote Sens. Environ. 22, 309–322.
Harron, J., Miller, J., 1995. An alternate methodology for reflectance and transmittance measurements of conifer needles. In: 17th Can. Symp. Remote Sensing, pp. 654–661.
Hovi, A., Mttus, M., Juola, J., Manoocheri, F., Rautiainen, M., 2020. Evaluating the performance of a double integrating sphere in measurement of reflectance, transmittance, and albedo of coniferous needles. Silva Fennica 54.
Hovi, A., Raitio, P., Rautiainen, M., 2017. A spectral analysis of 25 boreal tree species. Silva Fenn 51, 1–16.
Jacquemoud, S., Baret, F., 1990. PROSPECT: a model of leaf optical properties spectra. Remote Sens. Environ. 34, 75–91.
Jay, S., Gorretta, N., Morel, J., Maupas, F., Bendoula, R., Rabatel, G., Dutartre, D., Comar, A., Baret, F., 2017. Estimating leaf chlorophyll content in sugar beet canopies using millimeter-to centimeter-scale reflectance imagery. Remote Sens. Environ. 198, 173–186.
Lhotáková, Z., Albrechtová, J., Malenovský, Z., Rock, B.N., Polák, T., Cudlín, P., 2007. Does the azimuth orientation of Norway spruce (Picea abies/L./Karst.) branches within sunlit crown part influence the heterogeneity of biochemical, structural and spectral characteristics of needles? Environ. Exp. Bot. 59, 283–292.
Li, D., Tian, L., Wan, Z., Jia, M., Yao, X., Tian, Y., Zhu, Y., Cao, W., Cheng, T., 2019. Assessment of unified models for estimating leaf chlorophyll content across directional-hemispherical reflectance and bidirectional reflectance spectra. Remote Sens. Environ. 231, 111240.
Li, L., Mu, X., Qi, J., Pisek, J., Roosjen, P., Yan, G., Huang, H., Liu, S., Baret, F., 2021. Characterizing reflectance anisotropy of background soil in open-canopy plantations using UAV-based multiangular images. ISPRS J. Photogramm. Remote Sens. 177, 263–278.
Ling, C., Liu, H., Ju, H., Zhang, H., You, J., Li, W., 2017. A study on spectral signature analysis of wetland vegetation based on ground imaging spectrum data. In: Journal of Physics: Conference Series. IOP Publishing, 012045.
Lukeš, P., Stenberg, P., Rautiainen, M., Mottus, M., Vanhatalo, K.M., 2013. Optical properties of leaves and needles for boreal tree species in Europe. Remote Sens. Lett. 4, 667–676.
Malenovský, Z., Albrechtová, J., Lhotáková, Z., Zurita-Milla, R., Clevers, J., Schaepman, M.E., Cudlín, P., 2006. Applicability of the PROSPECT model for Norway spruce needles. Int. J. Remote Sens. 27, 5315–5340.
Mesarch, M.A., Walter-Shea, E.A., Asner, G.P., Middleton, E.M., Chan, S.S., 1999. A revised measurement methodology for conifer needles spectral optical properties: evaluating the INFLUENCE OF GAPS BETWEEN ELEMents. Remote Sens. Environ.
Middleton, E.M., Chan, S.S., Rusin, R.J., Mitchell, S.K., 1997. Optical Properties of black spruce and jack pine needles at BOREAS sites in Saskatchewan, Canada. Can. J. Remote Sens.
Moorthy, I., Miller, J.R., Noland, T.L., 2008. Estimating chlorophyll concentration in conifer needles with hyperspectral data: an assessment at the needle and canopy level. Remote Sens. Environ. 112, 2824–2838.
Moorthy, I., Miller, J.R., Zarco-Tejada, P.J., Noland, T.L., 2004. Needle Chlorophyll Content Estimation: A Comparative Study of PROSPECT and LIBERTY.
Nicodemus, F.E., Richmond, J.C., Hsia, J.J., Ginsberg, I.W., Limperis, T., 1977. Geometrical Considerations and Nomenclature For Reflectance. National Bureau of Standards, US Department of Commerce, Washington, DC.
O'neill, A., Kupiec, J., Curran, P., 2002. Biochemical and reflectance variation throughout a Sitka spruce canopy. Remote Sens. Environ. 80, 134–142.

Ramsey, E.W., Rangoonwala, A., 2004. Remote sensing and the optical properties of the narrow cylindrical leaves of juncus roemerianus. Geosci. Remote Sens. IEEE Trans. on 42, 1064–1075.
Rautiainen, M., Lukeš, P., Homolová, L., Hovi, A., Pisek, J., Mõttus, M., 2018. Spectral Properties of Coniferous Forests: a Review of In Situ and Laboratory Measurements. Remote Sens. (Basel.) 10, 207.
Schaepman-Strub, G., Schaepman, M.E., Painter, T.H., Dangel, S., Martonchik, J.V., 2006. Reflectance quantities in optical remote sensing—Definitions and case studies. Remote Sens. Environ. 103, 27–42.
Schlemmer, M., Gitelson, A., Schepers, J., Ferguson, R., Peng, Y., Shanahan, J., Rundquist, D., 2013. Remote estimation of nitrogen and chlorophyll contents in maize at leaf and canopy levels. Int. J. Appl. Earth Obs. Geoinf. 25, 47–54.
Shi, H., Xiao, Z., 2021. A canopy radiative transfer model considering leaf dorsoventrality. IEEE Trans. Geosci. Remote Sens. 60, 1–11.
Verhoef, W., 1984. Light Scattering by Leaf Layers with Application to Canopy Reflectance Modeling: The SAIL Model, 16. Remote Sensing of Environment, pp. 125–141.
Wang, J., Chen, J.M., Feng, L., Xu, J., Zhang, F., 2020. Redefining the directional-hemispherical reflectance and transmittance of needle-shaped leaves to address issues in their existing measurement methods. Photogram. Eng. Remote Sens. 86, 627–641.
Yanez-Rausell, L., Malenovsky, Z., Clevers, J., Schaepman, M.E., 2014a. Minimizing measurement uncertainties of coniferous needle-leaf optical properties. Part II: experimental setup and error analysis. IEEE J Sel Top Appl Earth Obs Remote Sens 7, 406–420.
Yanez-Rausell, L., Schaepman, M.E., Clevers, J., Malenovsky, Z., 2014b. Minimizing measurement uncertainties of coniferous needle-leaf optical properties, Part I: methodological review. IEEE J. Sel. Top. Appl. Earth Obs Remote Sens 7, 399–405.
Zhang, L., Sun, X., Wu, T., Zhang, H., 2015. An analysis of shadow effects on spectral vegetation indexes using a ground-based imaging spectrometer. IEEE Geosci. Remote Sens. Lett. 12, 2188–2192.
Zhang, N., Pan, Y., Feng, H., Zhao, X., Yang, X., Ding, C., Yang, G., 2019. Development of Fusarium head blight classification index using hyperspectral microscopy images of winter wheat spikelets. Biosyst. Eng. 186, 83–99.
Zhang, Y., Chen, J.M., Miller, J.R., Noland, T.L., 2008. Retrieving chlorophyll content in conifer needles from hyperspectral measurements. Can. J. Remote Sens. 34, 296–310.